Chaos in trapped particle orbits

R. B. White
Plasma Physics Laboratory, Princeton University, P.O. Box 451, Princeton, New Jersey 08543
(Received 9 January 1998; revised manuscript received 25 March 1998)

An analytic expression is obtained for the threshold for stochastic transport of high energy trapped particles in a tokamak due to toroidal field ripple. The result permits a rapid evaluation of energetic particle loss in general equilibria. The approach to chaos has two limiting cases: island overlap from neighboring precession resonances, and the overlap of bounce resonance webs extending from resonant surfaces. In both cases the physical resonance consists of motion through a distance which is an integer multiple of the field coil separation in one bounce. [S1063-651X(98)13608-5]

PACS number(s): 05.45.+b, 52.55.Dy, 52.20.Dq

I. INTRODUCTION

In magnetic fusion devices, the long time confinement of high energy particles, whether 3.5 MeV alpha particle fusion products or other ions introduced for heating purposes, is essential to the attainment of a self sustaining nuclear burn. It has been well established that the motion of such particles, with energies much higher than the typical 10-keV background plasma, is neoclassical [1]. That is, small scale fluctuations present in plasmas, and thought to be responsible for the anomalous thermal flux to the plasma edge, do not influence the orbits. Thus their motion is that of charged test particles in a given magnetic field. Nevertheless, predicting the degree of alpha particle confinement in a given device with high accuracy requires many hours of computing time, even using algorithms in which the rapid gyro motion has been eliminated. This is because there are vastly differing time scales for the three major contributing loss processes. The slower loss processes correspond to the nonconservation of an integral of the motion, and thus of a broken symmetry of the underlying Hamiltonian describing the dynamics. The simplest description is given by a toroidally symmetric equilibrium, with neglect of particle-particle interactions.

Any axisymmetric equilibrium field can be expressed in contravariant and covariant forms [2,3]

$$\vec{B}_0=\vec{\nabla}\zeta\times\vec{\nabla}\Psi_p+q(\Psi_p)\vec{\nabla}\Psi_p\times\vec{\nabla}\theta, \tag{1}$$

$$\vec{B}_0=g(\Psi_p)\vec{\nabla}\zeta+I(\Psi_p)\vec{\nabla}\theta+h(\Psi_p,\theta)\vec{\nabla}\Psi_p, \tag{2}$$

with Ψ_p the poloidal flux, θ the poloidal angle, and ζ a toroidal angle. The coordinate system is a straight field line one, i.e., $q(\Psi_p)$ (the safety factor) gives the local helicity of a field line $q=d\zeta/d\theta$, and also relates the toroidal flux Ψ and the poloidal flux Ψ_p, through $q=d\Psi/d\Psi_p$. The variable ζ is related to the geometric toroidal angle ϕ through $\zeta=\phi+\nu$, with ν a function of Ψ_p and θ, periodic in θ. The magnetic field strength $B_0(\Psi_p,\theta)$ is independent of the coordinate ζ. It is important to use general magnetic coordinates so that results will be applicable to any equilibrium, but for purposes of visualization Ψ_p may simply be regarded as the minor radius of the torus.

Guiding center motion in a field B is given by a Hamiltonian formalism [3–5]

$$\frac{dP_\zeta}{dt}=-\partial_\zeta\mathcal{H}, \quad \frac{d\zeta}{dt}=\partial_{P_\zeta}\mathcal{H}, \tag{3}$$

$$\frac{dP_\theta}{dt}=-\partial_\theta\mathcal{H}, \quad \frac{d\theta}{dt}=\partial_{P_\theta}\mathcal{H}, \tag{4}$$

where $P_0=I\rho_\parallel+\Psi$ and $P_\zeta=g\rho_\parallel-\Psi_p$ are the canonical momenta with $\rho_\parallel=v_\parallel/B$, and

$$\mathcal{H}=\frac{1}{2}\left(\frac{P_\zeta+\Psi_p}{g}\right)^2B^2+\mu B \tag{5}$$

is the Hamiltonian. Here and in the following we use units given by the on-axis gyro frequency (time) and the major radius (distance). In these units $\rho=\sqrt{2E}$ is the gyro radius, which is the small parameter in the guiding center approximation. A very important feature of these equations is that motion is given by $B(\Psi_p,\theta)$, the field magnitude only, and real space (metric) quantities such as the Jacobian do not enter.

Toroidal symmetry implies that P_ζ is a constant of the motion, and hence $\mathcal{H}=E$ implies that all orbits are closed curves in the Ψ_p,θ plane. By conservation of energy, orbits are restricted to connected regions of space in which $E\geqslant\mu B$. Normally the magnetic field decreases outwardly and thus there are orbits which are trapped poloidally and execute banana-shaped orbits. Although orbits close in the Ψ_p,θ plane they do not close in space, but precess toroidally. Because of the toroidal precession the banana tips describe constant Kolmogorov-Arnold-Moser (KAM) surfaces [6] in the Ψ_p,ϕ plane.

It is easy to perform a Monte Carlo calculation to determine the prompt, or first, orbit loss, due to orbits which intersect the outer boundary, the only loss process present with an axisymmetric equilibrium, typically occurring on a time scale of microseconds.

The most important symmetry breaking term to include in the Hamiltonian is due to the perturbation of the magnetic field strength due to the N toroidal field coils. It can be represented by a modulation of the field amplitude

$$B(\Psi_p,\theta,\phi)=B_0(\Psi_p,\theta)[1+\delta\cos(N\phi)], \tag{6}$$

with the ripple strength δ a function of position, determined by the coil geometry, and in all devices $N\gg1$.

These small modulations of the field amplitude have a significant effect only on poloidally trapped particles, and only near the banana tips. Premature or late bounce causes the banana tip to be shifted in Ψ_p, θ, and ϕ while conserving both E and μ. When the toroidal precession in one bounce is equal to an integer number of coil spacings, a period-1 resonance occurs, and the KAM surfaces describing the banana tips exhibit resonance islands. Growth of these islands, and that of smaller higher order islands, can lead to stochastic motion and particle loss. Loss of alpha particles or other high energy particles due to field ripple caused by the discrete toroidal field coils is an important consideration in the design of magnetic fusion tokamaks. It is also much more difficult to predict than prompt orbit loss. The time scale is typically on the order of milliseconds, so a full scale simulation requires significant computing.

The final symmetry breaking is due to particle-particle interaction, including pitch angle scattering, primarily from other ions, and drag, primarily from small angle scattering off electrons. If the system consists of high energy ions only, it is no longer even Hamiltonian, since the drag is dissipative. The time scale for this process is on the order of seconds. Since there are many orders of magnitude separating the orbital motion and the scattering, the scattering could be artificially enhanced, greatly reducing the computing, but such an enhancement interferes with the simulation of stochastic ripple induced loss. Thus an analytic evaluation of ripple loss can allow greatly improved simulations. This work extends previous approximate analyses [7,8] to obtain a complete expression for stochastic threshold.

II. BANANA TIP MAP

Axisymmetry, $\delta=0$, makes the toroidal canonical momentum P_ζ an integral of the motion, and this along with energy conservation means that all orbits are closed curves in the Ψ_p,θ plane. The banana tips describe constant KAM surfaces [6] in the Ψ_p,ϕ plane. The KAM theory guarantees that for small ripple this phase space changes topologically only in small regions where resonances produce islands. Stochastic threshold occurs in the manner described by Chirikov [6], with the destruction of the last remaining KAM surface allowing diffusion of an orbit leading to loss. To understand this process it is necessary to investigate resonances in the banana tip motion.

Consider the discrete map generated by a trapped particle, each step of the map corresponding to the banana tip position (Ψ_p,ϕ). Each half bounce the particle moves toroidally along the field, and in addition drifts across the field lines. The successive bounce points are given by the banana tip map [7,9–16].

$$\Psi_{p,t+1}=\Psi_{p,t}+\lambda\Delta\ \sin(N\phi_t), \tag{7}$$

$$N\phi_{t+1}=N\phi_t+N\phi_{b,t+1}+N\phi_{p,t+1}, \tag{8}$$

$$\Psi_{p,t+2}=\Psi_{p,t+1}+\Delta\ \sin(N\phi_{t+1}), \tag{9}$$

$$N\phi_{t+2}=N\phi_{t+1}-N\phi_{b,t+2}+N\phi_{p,t+2}, \tag{10}$$

where λ is a measure of up-down asymmetry; and $\phi_b=q\theta_{b+}+q\theta_{b-}$, with $\theta_{b\pm}$ the magnitudes of the poloidal bounce angles at the lower and upper banana tips, $\Psi_{p,t}$, ϕ_t the initial position of the bounce point at the lower banana tip, and ϕ_p is the toroidal precession of the banana tip during one half bounce. The first equation describes the change of flux surface due to ripple at the lower bounce point, the second equation the toroidal motion between the lower and upper bounce points, etc. The displacement amplitude is [17–19,5]

$$\Delta=\frac{g\rho\delta\sqrt{\pi Nq}}{B(\partial_\theta B/B)^{1/2}}. \tag{11}$$

These expressions are the result of integrating the drift equations in general magnetic coordinates, so of course include the effects of equilibrium shape. The only essential approximation made is that the dominant contribution of the ripple occurs near the banana tips.

The total precession during one half bounce in the straight field line variable ζ is easily seen to be the same as precession in the toroidal variable ϕ, and is given [5] by $\phi_p=\rho P(\Psi_p)$, with P a geometry-dependent integral independent of gyro radius,

$$P(\Psi_p)=\int_{-\theta_{b-}}^{\theta_{b+}}d\theta\left[\frac{g\rho_\parallel q'}{\rho}+\frac{\rho_\parallel(I'+qg')}{\rho}-\frac{(\mu+\rho_\parallel^2B)(I+gq)\partial_{\Psi_p}B}{\rho\rho_\parallel B^2}\right], \tag{12}$$

where $\rho_\parallel=\sqrt{2E-2\mu B}/B$, and primes refer to derivatives with respect to Ψ_p.

For reference only, in a large aspect ratio circular equilibrium this expression simplifies to $\phi_p\simeq 2\sqrt{2}(\rho/R)q^2(R/r)^{3/2}[2E(k)-K(k)]$ with $k=\sin(\theta_b/2)$, where E and K are elliptic integrals, and $d\Psi_p=rdr/q$.

The map thus depends on the functions of position ϕ_p, ϕ_b, Δ, and λ, which contain all the essential information about the particle precession and bounce motion, the equilibrium and the field ripple. Note that with up-down symmetry ($\lambda=1$) this map is *almost* a composition of two steps of the standard map [6]. Only the sign change of ϕ_b in Eq. (10) makes this not so, but this simple sign change has profound consequences for the way in which stochastic threshold is approached. In Fig. 1, is shown the trajectory of a trapped particle in the space of θ and ϕ. The precession motion ϕ_p and the bounce motion ϕ_b are indicated. The two crossed boxes on the left indicate magnetic field coils, and a precession resonance is shown consisting of precession of one coil spacing in one bounce.

III. FIXED POINTS

Now we search the banana tip map for fixed points, which are the *x* and *o* points of resonances. Approximate ϕ_b and ϕ_p as linear functions in Ψ_p, a simplification certainly valid over the scale of the resonance spacing. Conservation of energy E and magnetic moment μ makes the bounce angle in the unperturbed orbit a function of Ψ_p through $E=\mu B(\Psi_p,\theta_b)$, and thus $\phi_b'=q'\theta_{b+}+q'\theta_{b-}-q\partial_{\Psi_p}B/\partial_\theta B_+-q\partial_{\Psi_p}B/\partial_\theta B_-$. The derivative of ϕ_p must be evaluated using Eq. (12). We wish to identify all fixed points, calculate island widths at the resonant flux surfaces, and identify conditions for stochastic threshold. The total

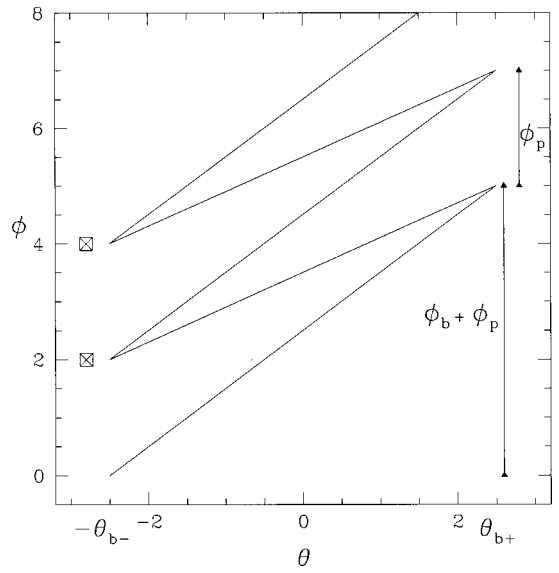

FIG. 1. Trapped particle trajectory showing precession resonance.

change in the position of the upper banana tip in one bounce is given by

$$d\Psi_p = \lambda\Delta\ \sin(N\phi) + \Delta\ \sin(z) \tag{13}$$

and

$$d\phi = 2\phi_p + 2\phi_p'\lambda\Delta\ \sin(N\phi) + (\phi_p' - \phi_b')\Delta\ \sin(z), \tag{14}$$

where $z = N\phi + 2w + 2w'\lambda\Delta\ \sin(N\phi)$, and $w = N\phi_b/2 + N\phi_p/2$.

The fixed points of the map are qualitatively different for different values of ϕ_p' and ϕ_b'. Refer to the flux surfaces $\phi_p = k\pi/N$ as precession resonance surfaces. These are surfaces at which the trapped particles considered (fixed values of Ψ_p, E, and θ_b) precess an integer number of coil spaces in one bounce. Let $\Psi_p = \Psi_{p,k} + \psi$, with $\Psi_{p,k}$ a precession resonance surface, the neighboring surfaces being located at $\psi = \pm\pi/(N\phi_p')$. This spacing is typically a small fraction of the minor radius, there can be as many as 100 resonances across the plasma. Period-1 fixed points are given by

$$\lambda\ \sin(N\phi) + \sin(z) = 0, \tag{15}$$

$$N\phi_p'\psi - w'\Delta\ \sin(z) = 0, \tag{16}$$

with $w = w_k + w'\psi$, and the subscript k indicating evaluation at the precession resonance surface $\psi = 0$.

Expanding Eqs. (13) and (14) around fixed points ψ_0 and ϕ_0, we find, for one bounce,

$$\begin{pmatrix} d\psi \\ d\phi \end{pmatrix} = \begin{pmatrix} M_{11} & M_{12} \\ M_{21} & M_{22} \end{pmatrix} \begin{pmatrix} \psi - \psi_0 \\ \phi - \phi_0 \end{pmatrix}, \tag{17}$$

with the matrix elements $M_{11} = 2w'\Delta\ \cos z_0$,

$$M_{12} = \lambda\Delta\ \cos N\phi_0 + \Delta\ \cos z_0 + 2\lambda\Delta^2 w' \cos z_0\ \cos N\phi_0,$$

$$M_{21} = 2\phi_p' + 2w'\Delta(\phi_p' - \phi_b')\cos z_0,$$

$$M_{22} = 2\phi_p'\lambda\Delta\ \cos N\phi_0 + (\phi_p' - \phi_b')\Delta\ \cos z_0 + 2w'\lambda\Delta^2(\phi_p' - \phi_b')\cos N\phi_0\ \cos z_0.$$

The determinant of M is positive at an elliptic fixed point, and negative at a hyperbolic fixed point.

If the term in Δ is negligible in Eq. (16) and in z, only $\psi \simeq 0$ is a solution, i.e., the only resonances are the precession resonances, and $N\phi$ and $N\phi - \pi$ are both solutions to Eq. (15); the x and o points are separated by π, and $\det M \simeq -2\phi_p'\Delta[\lambda\ \cos N\phi + \cos(N\phi + 2w_k)]$. Physically the particle precesses through an integer number of field coils in one bounce, with the forward and backward movement due to the bounce motion cancelling out.

Increasing the term in Δ initially simply modifies the position of the precession resonances, but there are additional solutions to Eqs. (15) and (16) if this term is sufficiently large. Eliminating ψ we find a transcendental equation for z,

$$\frac{2(z - N\phi - 2w_k)}{N\phi_p'\Delta[1 - (\phi_b'/\phi_p')^2]} + \sin\ z = 0. \tag{18}$$

A sufficient condition for the existence of extra solutions is readily found by regarding $N\phi$ and w_k as unknown constants. There are multiple solutions to this equation for any values of $N\phi$ and w_k when the slope of the line is less than $2/(3\pi)$, or $N\phi_p'\Delta|1 - (\phi_b'/\phi_p')^2| > 3\pi$. Similarly a transcendental equation for ϕ can be found:

$$\frac{2(N\phi - z + 2w_k)}{N\phi_p'\Delta\lambda[1 - (\phi_b'/\phi_p')^2]} + \sin\ N\phi = 0. \tag{19}$$

Regarding z and w_k as unknown constants, a second condition for the existence of extra solutions is found. Again multiple solutions exist when the slope of the line is less than $2/(3\pi)$, or $N\phi_p'\Delta\lambda|1 - (\phi_b'/\phi_p')^2| > 3\pi$. The value of λ determines which of these equations is least restrictive. Of course the extra solutions are identical, whether considered in ϕ or z, and if one sufficient condition for solution is satisfied then extra solutions exist also in the other variable.

The exact locations can only be obtained numerically, but treating $N\phi$, z as random variables in Eqs. (15) and (16), two upper bounds on the extent of the solutions can be found. Since each condition is a strict upper bound the stronger condition determines the extent. The envelope of the domain of additional solutions is given by $|\psi| \leqslant \psi_w$, with

$$\psi_w = |1 - \phi_b'/\phi_p'|\Delta\ \min(1,\lambda)/2 \tag{20}$$

with the solution spacing given by $d\psi = \pi/(N\phi_p' + N\phi_b')$. As ϕ_b' increases the spacing approaches the bounce resonance spacing, and more and more bounce resonances appear on each side of each precession resonance. Also, as is clear from Eqs. (18) and (19), when many solutions exist, their extent is accurately given by ψ_w, with an error of one solution spacing.

Physically, note that the change in toroidal position due to the bounce motion in one bounce is $\phi_b(\psi_{t+1}) - \phi_b(\psi_{t+2}) \simeq -\phi_b'\Delta\ \sin(N\phi_{t+1})$. For small Δ this can have no significant effect, but when $\phi_b'\Delta$ is large enough this term can correct the resonance mismatch caused by distance from the precession resonance surface $\psi = 0$. Away from $\psi = 0$ the precession resonance is mismatched by a toroidal angle $\phi_p'\psi$, and thus when $\phi_b'\Delta \simeq \phi_p'\psi$ the bounce term can cause a new resonance to occur at a location $\psi \simeq \phi_b'\Delta/\phi_p'$, in agreement with Eq. (20). Farther away from the precession

resonance surface the bounce term is incapable of repairing the precession resonance mismatch. These additional resonances could thus be called ''bounce variation assisted precession resonances.'' However, all period-1 resonances consist of particle motion through an integer number of field coils in one bounce, whether achieved simply through precession or with the assistance of the gradient of the bounce term.

These are all the period-1 fixed points of the map. Now we turn to a discussion of the islands appearing around them.

IV. PRECESSION ISLANDS

To estimate stochastic threshold, it is necessary to calculate island widths and compare them to separation. The Chirikov overlap condition typically gives an amplitude too large for stochastic threshold [20], as actual threshold occurs when the island width is approximately a fraction $2/\pi$ of the resonance spacing. The resulting correction is sometimes referred to as the 2/3 rule [21], although more accurately it is the $2/\pi$ rule. It is due to the effects of higher order islands and to distortion of the KAM surfaces by the low order islands.

In the vicinity of a resonance, Eqs. (13) and (14) can be used to calculate the island width. If the distance from the resonance surface is small, and Δ is small enough so that the map is very far from stochastic threshold, then the steps in ψ and ϕ are very small, and the slope of the local KAM surface traced out by the map is approximately given by $d\psi/d\phi$ treated as differentials. It is readily verified numerically that integrating the resulting differential equation for ψ as a function of ϕ correctly reproduces the island structure of the map. The solution to the differential equation is of course not chaotic, and only valid in the vicinity of the particular resonance where the integration is made. This technique works on all maps, and can be successfully used to calculate island widths for the purpose of estimating stochastic threshold. For $\phi_b'\Delta, \phi_p'\Delta \ll 1$, and assuming a small variation in w, this differential equation can be integrated to give a description of a precession resonance

$$(N\phi_p'\psi)^2 = N\phi_p'[c - \lambda\Delta\ \cos(N\phi) - \Delta\ \cos(N\phi + 2w_k)], \tag{21}$$

from which the value $c = \lambda\Delta\ \cos(N\phi_x) + \Delta\ \cos(N\phi_x + 2w_k)$, with ϕ_x the x point, gives the separatrix. Using Eq. (15) and $N\phi_o = N\phi_x + \pi$, the island extent at the o point ϕ_o is given by $N\phi_p'\psi = \pm\sqrt{2N\phi_p'\Delta}[1 + \lambda^2 + 2\lambda\ \cos(2w)]^{1/4}$. Using the $2/\pi$ rule to estimate the threshold, we find for threshold due to precession motion

$$\Delta_p = \frac{2}{N\phi_p'}\left[\frac{1}{D_k^{1/4} + D_{k+1}^{1/4}}\right]^2, \tag{22}$$

with $D_k = 1 + \lambda^2 + 2\lambda\ \cos(2w_k)$, $w_{k+1} = w_k + \pi(1 + \phi_b'/\phi_p')/2$. This reduces approximately to Eq. (22) of White *et al.* [8] for $\lambda = 1$, and only in this case there is an infinity at $\phi_b'/\phi_p' = \pm 1$ and $w_k = \pi/2$. Although large Δ is not within the spirit of the analysis, this result is correct; the map can be easily seen to possess no islands for these parameter values for any value of Δ. Note that $\lambda^2 D_k(1/\lambda) = D_k(\lambda)$ makes the result symmetric in the two bounce tips.

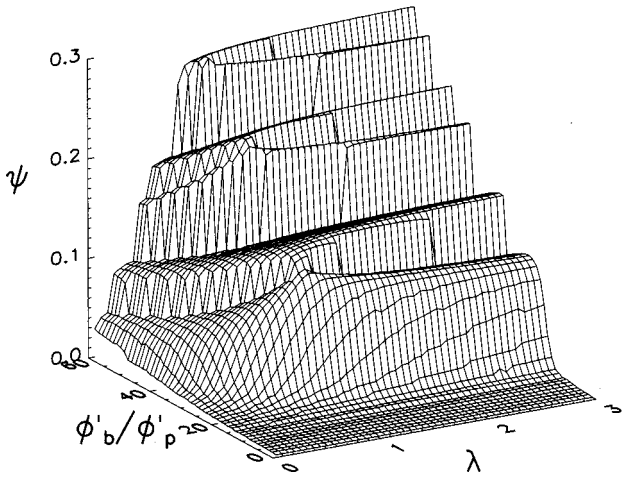

FIG. 2. Maximum extent of fixed points: $\Delta = 0.01$ and $w_k = 0$.

V. BOUNCE RESONANCE WEB

However, if the extent of the bounce resonances is comparable to the precession resonance spacing, the results are very different, and the approach to stochastic threshold is dominated by the generation of bounce resonance islands. In the limit $|\phi_b'/\phi_p'| \gg 1$ the map can again be analytically integrated. In this limit $w' = N\phi_b'/2$, $\psi_w = \infty$, and Eqs. (13) and (14) become $d\psi = [\lambda\Delta\ \sin(n\phi) + \Delta\ \sin(N\phi + 2w)]$ and $d\phi = -\phi_b'\Delta\ \sin(N\phi + 2w)$. Again consider continuous curves with slope $d\psi/d\phi$ given by the ratio of these small steps. The resulting differential equation is integrable with solution

$$\cos(N\phi + 2w) + \lambda\ \cos(N\phi) = K. \tag{23}$$

This equation describes a web with internal structure determined by the bounce resonance spacing, independent of ripple. This is a multi-island structure which does not possess good KAM surfaces prohibiting motion in ψ. For finite ψ_w the structure is well described by Eq. (23) only near $\psi = 0$, but the first good KAM surface is for $\psi > \psi_w$. In this respect it can be treated as an island structure, and used to calculate the stochastic threshold. Again we use the $2/\pi$ rule to determine threshold. We then find, from web overlap, the stochastic threshold due to bounce motion

$$\Delta_b = \frac{2}{|N\phi_b' - N\phi_p'|\min(\lambda, 1)}. \tag{24}$$

Previously [8], the threshold in the limit of large ϕ_b' and $\lambda = 1$ was numerically determined to be $2/(N\phi_b')$, in agreement with this estimate. Notice that the extent of the web is linear in Δ, as opposed to the square root dependence of precession island width.

VI. DEVELOPMENT OF THE WEB

The transition region from precession islands to web is best observed for small Δ, so that precession islands are small and well separated and higher order islands are very small. In Fig. 2 is shown the maximum extent of the fixed points as a function of λ and ϕ_b' for $\Delta = 0.01$, $N\phi_p' = 1$, and

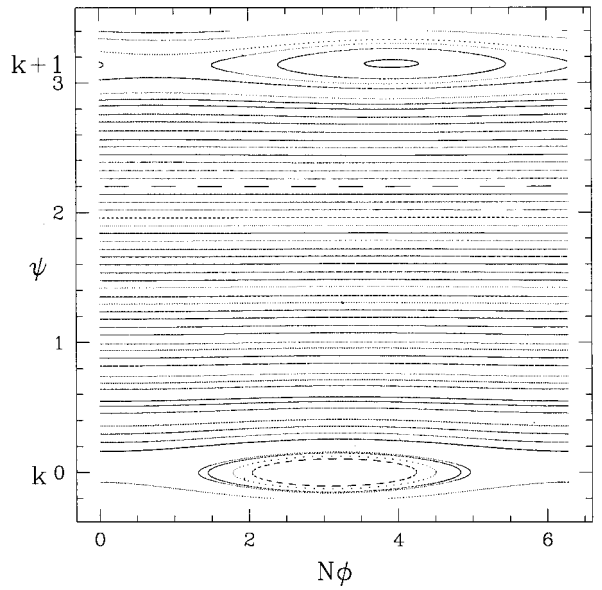

FIG. 3. Poincaré plot: $\Delta=0.01$, $N\phi_p'=1$, $w_k=0$, and $N\phi_b'=0.5$.

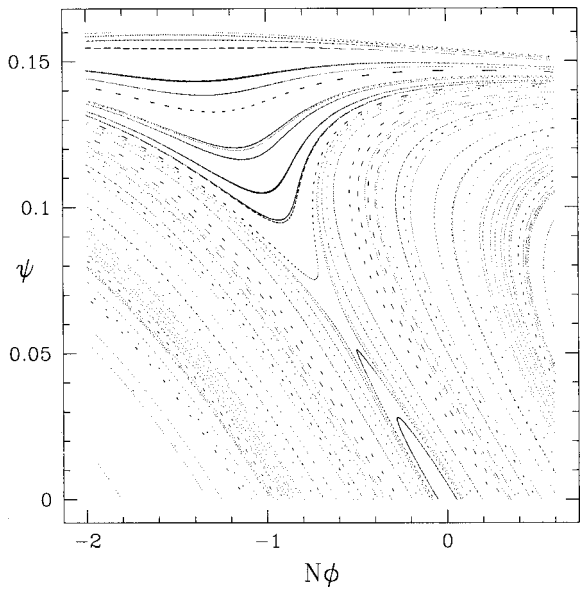

FIG. 5. Poincaré plot: $\Delta=0.01$, $N\phi_p'=1$, $w_k=0$, and $N\phi_b'=20.5$.

$w_k=0$, which is bounded by the value ψ_w. In Figs. 3–7 are shown Poincaré maps for the same parameters with $\lambda=1$, with increasing values of ϕ_b'. We have chosen $\lambda=1$ because Eq. (15) can then be solved analytically. Figures 3 and 4 show the primary islands for small ϕ_b'. Although Eqs. (13) and (14) cannot be used to find all fixed points analytically, the initial modification of the precession islands as ϕ_b' increases can be derived. Equation (15) has two solutions. First $z=-N\phi+2\pi l$, 1 integer, for which Eq. (16) becomes $f_l(\phi)=0$ with

$$f_l(\phi)=N\phi+[1-(\phi_b'/\phi_p')^2](N\phi_p'\Delta/4)\sin(N\phi)-\pi l. \tag{25}$$

For small ϕ_b' there is a single solution to $f_0=0$, but for $N\phi_p'\Delta|1-(\phi_b'/\phi_p')^2|=4$ there is a bifurcation at $\phi=0$, with $f_0=f_0'=f_0''=0$, and for larger values of ϕ_b' there are three real roots to the equation. Also at this value ($N\phi_b'\simeq 20$ for these parameter values) the determinant of the matrix M changes from negative to positive at $\phi=0$, and the x point at 0,0 becomes an o point surrounded by two x points. In Fig. 5 ($N\phi_b'=20.5$), a narrow island at the original x point ($\psi=0$, $\phi=0$) is just visible, and new x points have formed at $\psi=\pm 0.06$. This bounce resonance phenomenon was previously mistakenly interpreted as a nonlinear period doubling [8].

Second, we can observe the threshold for the formation of the first bounce resonance away from $\psi=0$. The second solution of Eq. (15) is $z=N\phi+\pi+2\pi l$. Equation (16) then gives $g_l(\phi)=0$, with

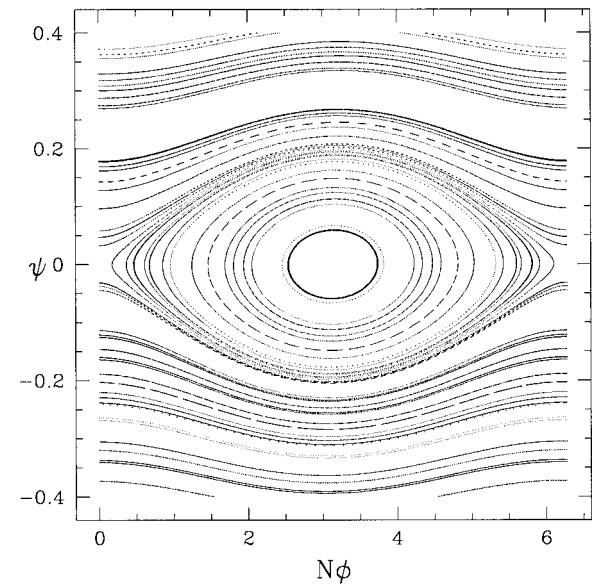

FIG. 4. Poincaré plot: $\Delta=0.01$, $N\phi_p'=1$, $w_k=0$, and $N\phi_b'=0.5$.

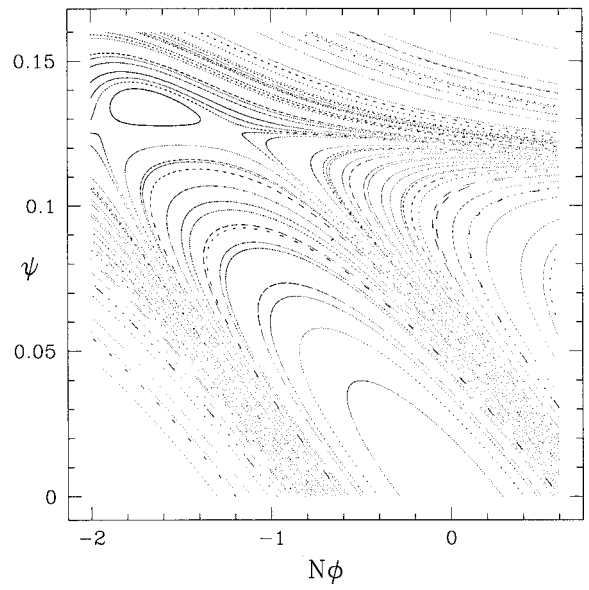

FIG. 6. Poincaré plot: $\Delta=0.01$, $N\phi_p'=1$, $w_k=0$, and $N\phi_b'=26$.

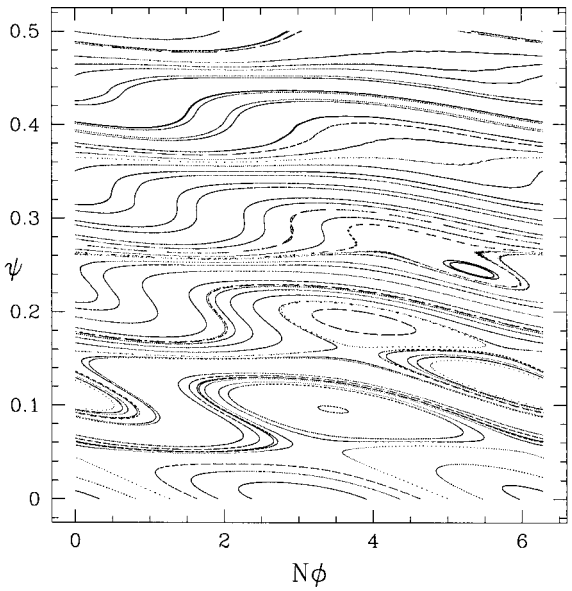

FIG. 7. Poincaré plot: $\Delta=0.01$, $N\phi_p'=1$, $w_k=0$, and $N\phi_b'=60$.

$$g_l(\phi)=N\phi_p'(\pi+2\pi l)/w'+(2w'-2N\phi_p')\Delta\ \sin(N\phi). \tag{26}$$

At $N\phi=-\pi/2$, for $N\phi_p'\Delta|1-(\phi_b'/\phi_p')^2|=2\pi$, ($N\phi_b'=25.07$) there is a triple root formed by f_0, g_0, and $g_0'=0$. At this confluence the f_0 root becomes an *o* point. In Fig. 6 ($N\phi_b'=26$), the *o* point is just visible at $\psi=0.135$, $N\phi=-1.6$, and the two *x* points from g_0 are at $\psi=0.122$ and $N\phi=-1.1$ and -1.9. The island at (0,0) has grown significantly. In Fig. 7 ($N\phi_b'=60$), the precession island has shrunk almost to the bounce resonance scale, and the web includes three layers of bounce resonance islands, extending to $\psi_w=0.3$. Near $\psi=0$ the web is very well formed, and given by Eq. (23). It is also interesting to note that in this limit the domain without good KAM surfaces is proportional to Δ, not $\sqrt{\Delta}$ as is usually the case.

VII. CONCLUSION

Examination of the fixed points and islands in the banana tip map results in a complete understanding of the approach to chaos. Chaotic orbits are produced either by the overlap of precession islands, or by the growth of a bounce resonance web. All resonances are due to particle precession through an integer number of field coils. An expression for stochastic threshold is then given by the smaller of Δ_p and Δ_b provided $N\phi_p'\max(\lambda,1)\Delta|1-(\phi_b'/\phi_p')^2|>3\pi$, otherwise by Δ_p. The transition from one expression to the other occurs when the extent of the bounce resonance web equals the precession island width. As has been shown previously, a good understanding of stochastic threshold allows the development of an algorithm for prompt axisymmetric orbit loss, ripple trapping, convective banana flow, and stochastic ripple loss, which can be extended to include the effects of collisions and drag, allowing rapid estimation of particle loss in tokamaks [8].

ACKNOWLEDGMENTS

The author is grateful to the Department of Physics at the University of California, Los Angeles, for hospitality during a brief visit during which a major part of this work was completed. This work was supported by the U.S. Department of Energy under Contract No. DE-AC02-76-CHO3073.

[1] S. J. Zweben, Plasma Phys. Controlled Fusion **39**, A275 (1997).
[2] A. H. Boozer, Phys. Fluids **24**, 1999 (1981).
[3] R. B. White and M. S. Chance, Phys. Fluids **27**, 2455 (1984).
[4] R. B. White, Phys. Fluids B **2**, 845 (1990).
[5] R. B. White, *Theory of Tokamak Plasma* (North Holland, Amsterdam, 1989).
[6] B. V. Chirikov, Phys. Rep. **52**, 263 (1979).
[7] R. J. Goldston, R. B. White, and A. H. Boozer, Phys. Rev. Lett. **47**, 647 (1981).
[8] R. B. White, R. J. Goldston, M. Redi, and R. V. Budny, Phys. Plasmas **3**, 3043 (1996).
[9] R. B. White, A. A. Boozer, R. Goldston, R. Hay, J. Albert, and C. F. F. Karney, Plasma Phys. Controlled Nucl. Fusion Res. **3**, 391 (1983).
[10] Y. I. Kolesnichenko and V. A. Yavorsky, in *Proceedings of the Sixteenth European Conference on Controlled Fusion and Plasma Physics Research* (European Physical Society, Venice, 1989), Vol. 13, p. 415.
[11] V. Y. Goloborodko and V. A. Yavorsky, in *Proceedings of the Sixteenth European Conference on Controlled Fusion and Plasma Physics Research* (Ref. [10]), p. 419.
[12] F. Zajtsev, A. P. Smirnov, and P. Yushmanov, Nucl. Fusion **26**, 1311 (1986).
[13] Y. I. Kolesnichenko and V. A. Yavorsky, Nucl. Fusion **29**, 1319 (1989).
[14] L. G. Eriksson and P. Helander, Nucl. Fusion **33**, 767 (1993).
[15] 'P. G. J. P. Roubin, Nucl. Fusion **30**, 1499 (1990).
[16] P. N. Yushmanov, Rev. Plasma Phys. **16**, 55 (1990).
[17] A. H. Boozer, Phys. Fluids **23**, 2283 (1980).
[18] R. J. Goldston and H. H. Towner, J. Plasma Phys. **26**, 283 (1981).
[19] P. N. Yushmanov, Nucl. Fusion **23**, 1599 (1983).
[20] J. M. Greene, J. Math. Phys. **20**, 1183 (1979).
[21] A. J. Lichtenberg and M. A. Lieberman, *Regular and Stochastic Motion* (Springer Verlag, Berlin, 1983), p. 292.